RSC Advances

ROYAL SOCIETY OF CHEMISTRY

www.rsc.org/advances

RSCPublishing

COMMUNICATION

A Three-dimensional Multilayered SiO-graphene Nanostructures as Superior Anode Material for Lithium-ion Batteries †

Cite this: DOI: 10.1039/x0xx00000x

Received ooth January 2012,
Accepted ooth January 2012

DOI: 10.1039/x0xx00000x

www.rsc.org/

Chenfeng Guo[a], Jingxuan Mao[b], Dianlong Wang[a]*

A Three-dimensional (3D) multilayered nanostructures to improve the electrode performance of SiO-based material through the use of reduced graphene oxide (RGO) film and Ni foam substrate has been developed. The lithium storage performance of the prepared anode is evaluated by electrochemistry measurements. The as-synthesized 3D SiO-RGO nanostrutures showed excellent electrochemistry properties as an anode in lithium-ion batteries.

Introduction

The decisive factor for the development of advanced lithium-ion batteries (LIBs) is the high-performance electrochemical properties of electrode materials, such as stability, conductivity, and Li^+ diffusion.[1-5] To meet these requirements, finding novel anode materials with improved performances is still under way. Compared with the graphite anode (commercial anode material), which has a limited theoretical specific capacity of 372 mA h g^{-1}, Silicon monoxide (SiO) has been proposed as one of most promising anode candidates for next-generation LIBs, owing to its significant high theoretical capacity was reported to be 2400 mAh g^{-1},[6] and low charge-discharge potential. However, the reported expansion percentage of SiO is still close to 200% of the initial volume during Li^+ insertion/extraction process, which is significantly larger than that of graphite negative electrode (1.1 times as large as the initial).[7] Various attempts to stabilize this structure have been reported. The most common attempt is to encapsulate the SiO structure with a conducting carbonaceous layer, in hope that this would effectively retard the growth of Silicon (Si) crystal, which will favor Li^+ insertion/deinsertion due to the shortened distance.[8-11] A key role of carbonaceous materials in those types of SiO-based structure is that they can buffer the pulverization of SiO upon Li^+ insertion/ deinsertion.

Graphene, a single-atom-thick sheet of honeycomb carbon lattice, was discovered in 2004 and proved to be chemically stable and possess excellent electron conductivity.[12] Recently, various hybrid nanostructures containing graphene nanosheets have been designed as electrode materials.[13-17] In LIBs, graphene can be exploited by integrating it as a structural buffer in the anode that can withstand the enormous strains generated during charge/discharge process. Herein we propose and realize a novel SiO-based anode nanostructure, namely 3D SiO/RGO nanostructures, assembly of alternating SiO/RGO layers on porous Ni foam (Figure 1). This strategy integrates both 3D porous structure and RGO coating.

The novel synthetic nanostructures possess several advantages as LIB anodes. (1) The nano-scale characteristics of SiO particles ensures the fast Li-ion diffusion in the electrode; (2) due to its distinctive properties, RGO film which is tough and elastic enough to compensate the large volume change of the SiO nanoparticles (NPs), prevent the aggregation of SiO NPs; (3) The specific surface area of nickel foam is much higher than that of conventional thin foil, thus depositing anode materials on a nickel foam substrate is an attractive method to prepare anode electrodes for LIBs.[18, 19] The nanosized SiO particles, the interconnected RGO, the 3D porous structure of Ni foam and the preparation of binder- and conductive agent-free electrodes make it possible for obtaining exceptional high reversible specific capacity, ultra long cyclic life and superior high-rate capability as a result of the better electrical contacts between the active materials and the used current collectors.

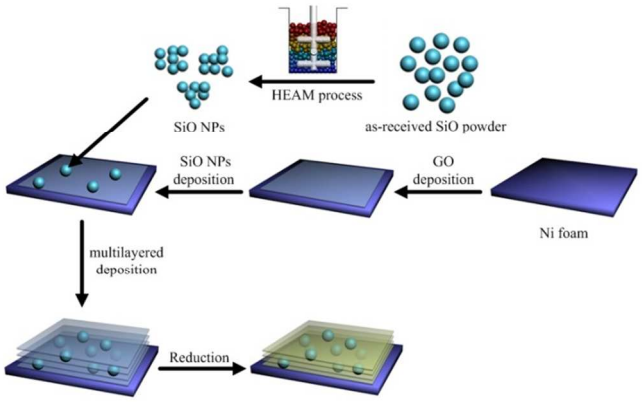

Figure 1. Illustration of the preparation process and microstructure characteristics of 3D SiO-RGO nanostructures.

Experiment

Materials Synthesis

Figure. 1 illustrates the synthesis procedure for the 3D SiO-RGO nanostructures. The commercially available pristine SiO powders (Aldrich) with an average particle size of 40 μm was treated with high efficient attritor mill (HEAM) technique in a hardened steel vial

with zirconia balls in ethanol, using a 01-HD/HDDM Lab Attritor with intensive rotation speed at 2500 rpm for 2h. The resultant dark brown precipitate was dried at 60°C under vacuum conditions, then the SiO NPs was obtained. Graphene oxide (GO) was prepared from purified natural graphite according to Hummers method as previous reports.[44, 45] 3D SiO-RGO nanostructures were prepared via a facile dip-coating method modifying a procedure reported by Jingbo Chang[3] as follows: A Ni foam was immersed into a well-dispersed GO suspension in ethanol (1 mg mL^{-1}) to load certain amount of GO in the pores. Then the coated GO surfaces were dried by N_2 gas. The dried GO-coated Ni foam was then dipped in a bath of SiO NPs dispersion in ethanol (1 mg mL^{-1}) and dried with N_2 gas, too. Therefore, multilayered electrodes could be obtained using the repetition of dip-coating procedure by alternating deposition of GO and SiO NP layers (Figure1). After calcination at 650 °C for 2 h under reductive (5 vol.% of hydrogen in argon) atmosphere in a furnace, the 3D SiO-RGO nanostructures anode were obtained. The prepared multilayered SiO/RGO electrode consisted of 15-layer SiO NPs films and 20-layer GO films, and the total weight of the anode material was 0.30 mg. For comparison, 3D SiO was fabricated as follows: the Ni foam was dipped into an SiO NPs dispersion and then taken out for several times. The SiO NPs covered the entire Ni foam after drying and then multilayered 3D SiO electrode was obtained.

Materials Characterization

X-ray diffraction (XRD) patterns of the as-prepared materials were collected on a D/max-γB X-ray diffractometer (Rigaku, Japan) using Cu Kα radiation (λ=1.54178Å). Raman spectrum was acquired on a Jobin Yvon HR800 confocal Raman system with 632.81nm diode laser excitation. X-ray photoemission spectroscopy (XPS) measurements were performed on a spectrophotometer (PHI Quantera SXM) using the monochromatic AlKa radiation (1486.6 eV) to evaluate the elemental compositions and chemical status of the samples. FESEM analysis was performed on a Hitachi S-4700 equipped with EDAX. TEM and HRTEM analyses were performed on a JEM-2100F microscope with an accelerating voltage at 200kV. The content of RGO in 3D Sn-GNS was analyzed by Vario EL cube (Elementar, Germany). For elemental analysis, multilayered SiO-RGO film was carefully stripped off from Ni foam matrix, and burned to form carbon dioxide. According to the mass of carbon dioxide, the content of RGO in SiO-RGO could be established.

Electrochemical Measurement

Electrochemical performances of the as-prerared samples were investigated with a two-electrode coin-type cell (CR2025). Test cells were assembled in an argon-filled glove box with the as-prepared 3D SiO-RGO or 3D SiO nanostructures on foam nickel was used as the working electrode, the metallic lithium foil as both the reference and counter electrodes, 1 M $LiPF_6$ in ethylene carbonate (EC)-dimethyl carbonate (DME) (1:1 in volume) as the electrolyte, and a polypropylene (PP) micro-porous film (Cellgard 2300) as the separator. The cells were charged and discharged over a voltage range of 0.01-1.5V (vs. Li/Li^+) at different current rates which were independent of the testing procedure using a Battery Testing System (Neware, China). Cyclic voltammetry curves were measured at a scanning rate of 0.1 mV s^{-1} within the potential range of 0.01-3.0 V vs. Li/Li^+ using an electrochemistry working station (CHI660). The electrochemical impedance spectroscopy (EIS) test was carried out in the frequency range from 100 kHz to 10 mHz on an electrochemical workstation (CHI660). Note that, in the typical synthesis, the SiO-RGO active material in 3D SiO-RGO contains 22.9 wt.% of RGO and 77.08 wt.% of SiO according to the elemental analysis. The specific capacity values of the battery were calculated on the basis of the total weight of SiO and RGO. On the basis of the equation described below, we could calculate a theoretical capacity (Q) of the hypothetical mixture of SiO-RGO, as follows:

$Q_{theoretical}=Q_{SiO}\times$mass percentage of SiO$+Q_{Graphite}\times$mass percentage of RGO $=2400\times77.08\% + 372\times22.92\% = 1935.18$ mA hg^{-1}

(The theoretical capacity of SiO was calculated on the basis of theoretical capacity of SiO previously reported.[47])

Results and discussion

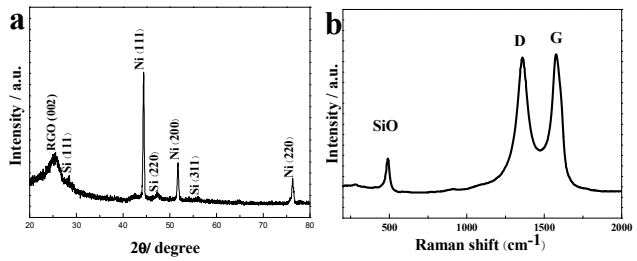

Figure 2. (a) X-ray diffraction pattern and (b) Raman spectrum of 3D SiO-RGO nanostructures.

Figure 2a shows the X-ray diffraction (XRD) pattern of the as-prepared 3D SiO-RGO nanostructures, in which all of the XRD peaks are in good agreement with the standard values of Si (JCPDS no.27-1402) and 002 planes of graphite excluding the peaks from the Ni foam substrate (JCPDS no.70-1849), which indicates the formation of SiO-RGO on Ni foam in the experiment. The Raman spectrum of 3D SiO-RGO (Figure 2b) displays a broad peak at around 490 cm^{-1}, which is in good agreement with the typical Raman mode of SiO,[20] and another two prominent peaks at around 1362 cm^{-1} and 1576 cm^{-1}, which are identified respectively as the D band and G band of RGO.[21] The result of Raman spectroscopy was employed to confirm further the SiO NPs and the existence of RGO in the 3D SiO-RGO. In Figure S1a, the X-ray photoelectron spectroscopy (XPS) result demonstrated three dominant elements corresponding to C (C 1s at 285 eV), Si (Si 2p at 102.6 eV) and O (O 1s at 534.6 eV). However, Ni element is undetected, which indicates the homogeneously dispersion of SiO-RGO on the surface of Ni foam. Figure S1b showed the high-resolution XPS Si 2p spectrum of 3D SiO-RGO, a strong peak at about 102.6 eV with a broad shoulder accounted for the unique Si chemical state (Si^{2+} from SiO).[22-24] In Figure S1d, the deconvoluted XPS C1s spectra of 3D SiO-RGO clearly indicated four components that are assigned to different functional groups: aromatic ring C (284.7 eV), C-O bond (286.5 eV) from overlapping of C-O-C and C-OH, C=O bond (287.8 eV), O-C=O group (288.2 eV).[25-27] The oxygen functionalities of the RGO are severely decreased in 3D SiO-RGO after the thermal reduction

process, which could be observed by comparing with the deconvoluted XPS C1s spectra of GO in previous reports.[25, 28, 29]

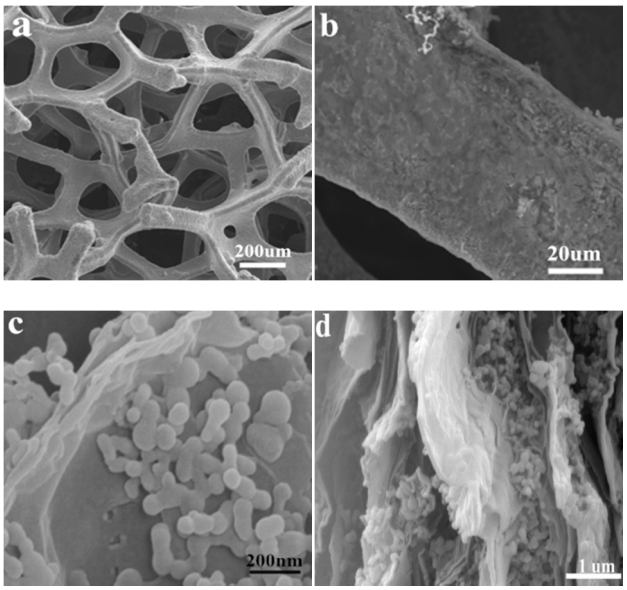

Figure 3. FESEM images of the 3D SiO-RGO nanostructures: (a) overview of the SiO/RGO nanostructure-coating 3D porous Ni foam; (b) low-magnification SEM image; (c) Top-view FESEM image; (d) Cross-section view FESEM image.

The structures of the 3D SiO-RGO nanostructure prepared with dip-coating method were characterized by FESEM, TEM and HRTEM respectively. The FESEM images of as-received SiO powder and SiO NPs are presented in Figure S2 a and b in order to compare their morphologies. The initial particle size of 40 μm was reduced to 50-150 nm by HEAM process. As depicted in Figure 3a and b, it can be seen that the SiO-RGO nanostructures are uniformly coated on the 3D porous Ni foam. Nickel foam is used here as an ideal electrode substrate, because of its high electronic conductivity, low weight, and 3D cross-linked grid structure, providing high porosity and surface area. Figure 3c shows an Top-view FESEM image of the multilayered 3D SiO/RGO nanostructures. At least three layers of SiO NPs could be identified with RGO layers in between. The cross-sectional FESEM image of the samples clearly shows multiple regularly spaced layers of SiO NPs separated by RGO film materials (Figure 3d). Layered nanostructures with alternating layers of SiO NPs and RGO stacks are also observed from TEM image (Figure S3a) of 3D SiO/RGO nanostructures. To further clarify the component and crystal structure of the SiO/RGO composite in 3D SiO-RGO nanostructure, the SiO/RGO composite was carefully scratched down from the Ni foam substrate and used for HRTEM characterization. HRTEM image (Figure S3b) of 3D SiO/RGO nanostructure showing the lattice fringes of Si along the (111) direction. Lattice fringes of 0.31 nm corresponding to (111) planes in crystal Si are marked. The HRTEM image also suggests 11 layers RGO with a thickness of approximately 4.7 nm. The disordered domain (indicated by green arrows) in the nanostructures should be amorphous SiO_x ($0 \le x \le 2$) microstructure. Energy dispersive X-ray analysis (EDAX) (Figure S4) also verifies the as-prepared 3D SiO/RGO material contains Si, O, Ni, and C elements with existence of element Si and O with approximately 1:1 ratio. This unique multilayered structure, the good contact between the SiO NPs and sandwiched RGO materials on the porous Ni foam, indicate that somewhat enhanced electrochemical performances of anode material in LIBs should be expected.

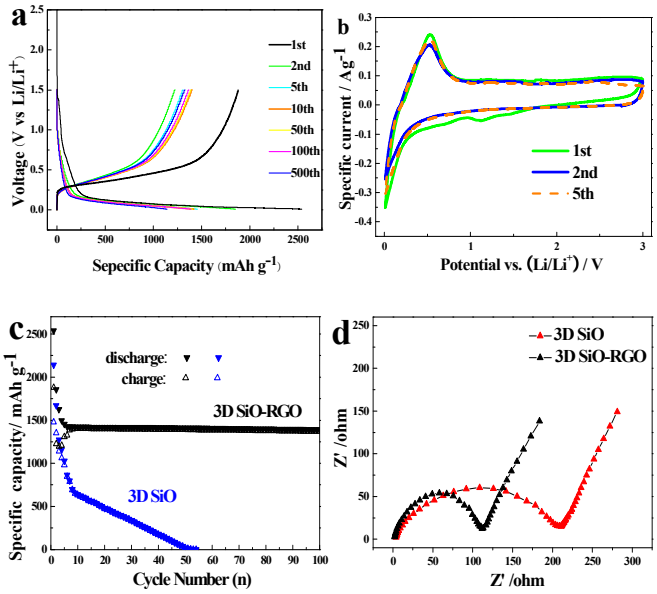

Figure 4. (a) Discharge-charge curves of 3D SiO/RGO cycled between 0 and 1.5 V under a current density of 100 mA g^{-1} for the 1st, 2nd, 5th, 10th, 50th, 100th and 400th cycle; (b) The CV curves of the3D SiO/RGO from the first cycle to the fifth cycle; (c) Cycling behaviors of 3D SiO/RGO and 3D SiO under a current density of 100 mA g^{-1}; (d) Nyquist plots of the electrodes of 3D SiO/RGO and 3D SiO.

The electrochemical performance of the 3D SiO/RGO nanostrutures was tested by galvanostatic discharge-charge technique. Typical charge-discharge profiles of 3D SiO-RGO nanostructure at a current density of 100 mA g^{-1} are shown in Figure 4a. The discharge-charge curves remain similar in shape, with a small decrease in the capacity from the 5th cycle to the 400th cycle. The initial discharge and charge specific capacities are 2539.7 and 1879.3 mA h g^{-1}, respectively, based on the total weight of SiO and RGO. The initial coulombic efficiency was calculated as high as 74%. The initial irreversible capacity loss should be attributed to the formation of solid electrolyte interphase (SEI) films on the surface of the electrode due to electrolyte decomposition[30] and irreversible Li^+ insertion into the nanostructure. Figure 4b shows CV curves of 3D SiO-RGO from the first cycle to the fifth cycle in the potential window of 0.01-3.0 V (vs. Li/Li^+). Three cathodic and one anodic current peaks for the 3D SiO-RGO electrodes could be observed in the 1st cycle. The reduction peak around 0.78 V and 1.21 V may be ascribed to the formation of SEI film on the 3D SiO-RGO, the reduction of SiO_2 to Si and the synchronous formation of Li_2O and Li_4SiO_4.[8] The cathodic peak at about 0.02 V corresponds to the formation of Li-Si alloy phases and the reversible reaction between Li and carbon.[31, 32] The pronounced peaks at 0.51 V at the anodic sweep could be ascribed to de-alloying of Li-Si alloys. In the following 2nd and 5th cycles, the CV curves are nearly overlapped, which indicates good stability of the 3D

SiO-RGO electrode from the 2nd cycle. The cycling performance of 3D SiO-RGO and 3D SiO were also studied, as shown in Figure 4c. It is found that 3D SiO-RGO shows the stable cycling performance, with a reversible capacity of 1369.5 mAh g^{-1} after 100 cycles, which is 3.6 times higher than the theoretical capacity of graphite. On the contrary, the 3D SiO electrode shows much faster capacity fading, up to 0% during 52 cycles. The reversible capacity of 3D SiO-RGO after 400 cycles is observed to be 1349.1 mAh g^{-1}, which is 96.1 % of the discharge capacity in the 10th cycle (Figure S6b). This result is comparable with or better than in previous reports, such as those on nano-sized SiO_x/C core-shell composite (800 mAh g^{-1}, 50 cycles),[10] nano-sized SiO_x (x=1.18)[33], disproportionation reaction of SiO and high energy mechanical milling modified SiO (close to 1000 mAh g^{-1}, 50 cycles)[34], N-doped carbon-coated SiO (955 mAh g^{-1}, 200 cycles)[35] ect. The robust structure of the 3D SiO-RGO is confirmed by the FESEM image of the sample after being used in LIBs for 100 cycles (Figure S5). As shown in the image, SiO NPs remain integrated with RGO film, showing that the electrode was not damaged by the cycling test. The rate performance of 3D SiO-RGO is shown in Figure S6a. The reversible capacities are 1316.3, 1135, 870.9, 671.5, 519.5 and 1355.4 mAh g^{-1} at the currents of 200, 400, 800, 1600, 3200 and back to 100 mA g^{-1}, respectively. These outstanding rechargeable capacities well exemplify the high rate capability offered by multilayered nanostructures and which are among one of the highest values so far reported for SiO-based electrodes.[8, 9, 35-41] Figure 4d shows the Nyquist plots of the 3D SiO-RGO and 3D SiO tested after 10 cycles. It could be clearly seen that the impedance spectra are almost similar in shape, composed of two semicircles at high and medium frequency ranges and followed by a linear part at the low frequency end. The semicircle in the high-frequency is associated with the SEI and contact resistance, and the semicircle in the medium frequency is attributed to the charge transfer impedance, and the inclined line corresponds to the frequency dependence of Li^+ diffusion/transport in the electrolyte.[42] It is obviously seen from Figure 4d that the size of the semicircle on the 3D SiO-RGO electrode is much smaller than that of the 3D SiO electrode, indicating lower charge transfer resistance. This result indicates that the 3D SiO-RGO electrode possesses a high electrical conductivity in comparison with the RGO-free 3D SiO electrode. The much improved electrochemical performance of 3D SiO-RGO electrode could be attributed to its unique electrode structure as following factors: (1) nanosized SiO particles shorten the transport path for both electrons and Li^+;[43] (2) the interconnected RGO could accommodate the volumetric change of SiO and facilitate the electron transfer of the active material; (3) the 3D porous structure of Ni foam ensures an even distribution of electrolyte in contact with the electrode surface. These structural characteristics finally lead to fast ion/electron transfer, sufficient contact between the active materials and electrolytes, and enhanced electrochemical properties.

Conclusions

In conclusion, we have presented a dip-coating fabrication method for preparing a 3D SiO-RGO nanostrutures, leading to multilayered sandwich structures by using a porous Ni foam as a substrate. The results from XRD, Raman, XPS, FESEM, EDAX, TEM and HRTEM proved that dip-coating fabrication was a feasible and reliable route to form layered alternating SiO/RGO nanostructures. The exceptional superior reversible specific capacity, cycling stability and high-rate capability of as synthesized material can be related to the positive influence of RGO, the small size of the SiO NPs and the 3D porous Ni foam current collector. The simple dip-coating fabrication approach, and the potential low manufacturing cost and binder-free properties may provide a new pathway for exploring 3D SiO-RGO nanostrutures as a promising anode material for high-energy and high-power LIBs. In addition, this preparation strategy is of potential interest to other high-capacity electrode materials with large volume variations and low electrical conductivities in the battery area.

Acknowledgement

We appreciate the support of National Natural Science Foundation of China (No. 50974045)

Notes and references

[a] *School of Chemical Engineering and Technology, Harbin Institute of Technology, Harbin, China. Fax: +86 451 86413721; Tel: +86 45186413751; E-mail: wangdianlonghit@163.com*

[b] *Harbin Engineering University, College of Software, Harbin 150001, P R China.*

† Electronic Supplementary Information (ESI) available: [details of any supplementary information available should be included here]. See DOI: 10.1039/b000000x/

1 K. T. Nam. *Science*, 2006, 312, 885.
2 J. M. Tarascon and M. Armand. *Nature*, 2001, 414, 359.
3 L. Taberna, S. Mitra, P. Poizot, P. Simon and J. M. Tarascon. *Nat. Mater*, 2006, 5, 567-573.
4 K. S. Kang, Y. S. Meng, J. Breger, C. P. Grey and G. Cefer. *Science*, 2006, 311.
5 B. Kang and G. Ceder. *Nature*, 2009, 458, 190.
6 Jae-Hun Kim, Cheol-Min Park, Hansu Kim, Young-Jun Kim and Hun-Joon Sohn. *Journal of Electroanalytical Chemistry,* 2011, 661, 245.
7 Beattie, S. D, Larcher, D, Morcrette, M, Simon, B and Tarascon, J. M. *J. Electrochem. Soc*, 2008, 155, A158.
8 Q. Si. et al. *J Power Sources,* 2011, 196, 9774.
9 Chil-Hoon Doh. et al. *J Power Sources*, 2008, 179, 367.
10 Jing Wang, Hailei Zhao, Jianchao He, Chunmei Wang and Jie Wang. *J Power Sources,* 2011, 196, 4811.
11 Xianxia Yuan, Ya-Jun Chao and Zi-Feng Ma. *Electrochem commun,* 2007, 9, 2591.
12 K.S. Novoselov. et al. *Science.* 2004, 306, 666.
13 Zhang, L. et al. *J. Mater. Chem*, 2010, 20, 5462.
14 Sun Y, Hu X, Luo W and Huang Y. *ACS Nano*, 2011, 5, 7100.
15 Guo, W. et al.*Energy Environ. Sci*, 2012, 5, 5221.
16 Li, B, Cao, H, Shao, J and Qu, M. *Chem. Commun*, 2011, 47, 10374.
17 Wang, B. et al. *J. Mater. Chem*, 2010, 20, 10661.
18 F. Gillot. et al. *Chem. Mater*, 2005, 17, 6327.
19 Y. Yu, C.H. Chen, J.L. Shui and S. Xie. *Angew. Chem. Int. Ed, 2005,* 44, 7085.
20 Leonid Khriachtchev, Sergei Novikov and Olli Kilpelä. *J. Appl. Phys,*

2000, 87, 7805.
21 Zhen-Huan Sheng. et al. *ACS Nano*, 2011, 5, 4350.
22 H.Kim, B.Han, J.Choo and J.Cho. *Angew. Chem., Int. Ed,* 2008, 47, 10151.
23 H.Kim, M.Seo, M.-H.Park and J.Cho. *Angew. Chem. ,Int. Ed*, 2010, 49, 2146.
24 N.Liu. et al. *Nano Lett,* 2012, 12, 3315.
25 O. Akhavan. *Carbon,* 2010, 48, 509.
26 A.V.Murugan, T. Muraliganth and A. Manthiram. *Chemistry of Materials*, 2009, 21, 5004.
27 J.X. Geng and H.T. Jung. *J. Phys. Chem. C*, 2010, 114. 8227.
28 Y.X. Xu, H. Bai, G.W. Lu, C. Li and G.Q. Shi. *Journal of the American Chemical Society,* 2008, 130, 5856.
29 S.J. Park, J.H. An, R.D. Piner, I. Jung and D.X. Yang, A. Velamakanni, S.B.T. Nguyen, R.S. Ruoff. *Chemistry of Materials*, 2008, 20, 6592.
30 Chan, C. K. Zhang, X. F. and Cui, Y. *Nano Lett,* 2008, 8, 307.
31 Peichao Lian. et al. *Electrochimica Acta*, 2010, 56, 834.
32 Xuyang Wang, Xufeng Zhou, Ke Yao, Jiangang Zhang and Zhaoping Liu. *Carbon*, 2011, 49, 133.
33 Min Kyung Kima, Bo Yun Jang, Jin Seok Lee, Joon Soo Kim and Sahn Nahm. *J Power Sources,* 2013, 244, 115.
34 Yoon Hwa, Cheol-Min Park and Hun-Joon Sohn. *J Power Sources,* 2013, 222, 129.
35 Dong Jin Lee, Myung-Hyun Ryou and Je-Nam Lee. *Electrochem. Commun*, 2013, 34, 98.
36 Mariko Miyachi, Hironori Yamamoto and Hidemasa Kawai. *J. Electrochem. Soc,* 2007, 154 (4), A376.
37 Toru Tabuchi, Hideo Yasuda and Masanori Yamachi. *J Power Sources,* 2005, 146, 507.
38 Shinichi Komaba. et al. *J. Phys. Chem. C,* 2011, 115, 13487.
39 T. Zhang. et al. *Electrochem commun*, 2007, 9, 886.
40 Xuejiao Feng, Jun Yang, Xiaolei Yu, Jiulin Wang and Yanna Nuli. *J Solid State Electrochem,* 2013, 17, 2461.
41 Byeong-Chul Yu, Yoon Hwa, Cheol-Min Park and Hun-Joon Sohn. *J. Mater. Chem. A*, 2013, 1, 4820.
42 C. Zhong, J. Z. Wang, Z. X. Chen and H. K. Liu. *J. Phys. Chem. C*, 115, 25115.
43 Dan Li, Xiuwan Li and Suiyan Wang. *ACS Appl. Mater. Interfaces*, 2014, 6, 648.
44 Lin Wang and Dian-Long Wang. *Electrochimica Acta,* 2011, 56, 5010.
45 Bo Wang. et al. *J. Mater. Chem. A*, 2013, 1, 135.
46 Jingbo Chang. et al. *Adv. Mater,* 2014, 26, 758.
47 Ya-Jun Chao, Xianxia Yuan and Zi-Feng Ma. *Electrochimica Acta,* 2008, 53, 3468.